# Unsteady Transonic Aerodynamics of Oscillating Airfoils in Supersonic Freestream

C. H. Wang,* D. K. James,* D. D. Liu†
*Arizona State University, Tempe, Arizona*
and
K. Y. Fung†
*University of Arizona, Tucson, Arizona*

**Nonlinear transonic/supersonic flows over an airfoil are studied comparatively using two computational codes, AZTRAN and TMOC, based on the small-disturbance theory. While AZTRAN is unified for all Mach numbers in the transonic regime, TMOC is restricted to the shock-attachment case. Computed results are verified with each other and with those of the ATRAN2 code, the linear theory, and other data whenever appropriate. Cases studied include inverse airfoil design, computation of pressure for an airfoil in pitching oscillations, and calculation of stiffness and damping moments. Finally, calculations of bending-torsion flutters according to linear and nonlinear theories are presented for a sharp and a blunt-leading-edge airfoil. Our findings indicate that the nonlinearity plays an essential role in this transonic regime.**

## Introduction

MODERN fighter aircraft are susceptible to aeroelastic instabilities in the low supersonic flow regime, i.e., $1.0 \leq M_\infty \leq 1.5$. When in maneuver at low altitude, the aircraft considered could be endangered by possible wing/tail or control surface flutter within its design flight envelope in this range.

Available measured data in this flow regime is rather limited. Because of the nonlinearity in this flow regime, only a few unsteady aerodynamic methods appear to be suitable for performing aeroelastic analysis, either in two or three dimensions. Although current supersonic panel methods such as Ref. 1 could yield accurate predictions in the supersonic regime, it might yield unsatisfactory results for thick airfoils in this nonlinear flow regime. Also, other earlier research efforts in the same flow regime were inconclusive (e.g., Refs. 2–5).

In recent years, almost all ongoing research efforts in unsteady transonics were focused on the subsonic freestream side. Little attention was given to its supersonic counterpart. For example, much research effort was devoted to the development of the XTRAN3S code for Mach numbers below 1. To address the aeroelastic concerns of fighter aircraft, it is essential to bridge the unsteady aerodynamic methodology from the subsonic regime through the supersonic regime.

The present work involves the investigation of the unsteady aerodynamic characteristics for several oscillating airfoils in this nonlinear supersonic flow regime. The objective of the present study is twofold. First, we present our newly developed two-dimensional transonic methods in this flow regime. Second, we provide a comprehensive study of existing two-dimensional approaches in order to validate the existing computer codes, as well as to establish benchmark checks for the later three-dimensional development. In fact, such a two-dimensional development forms the basic building block for our eventual three-dimensional unsteady transonic development, whose subsonic freestream counterpart, known as the transonic equivalent strip (TES) method,[6,7] has claimed much success in recent years.

## Present Developments

### Development of AZTRAN

The unsteady transonic code AZTRAN was developed for the subsonic freestream Mach numbers by Fung[8,9] at the University of Arizona and by Liu et al.[7] at Arizona State University in extending it for unsteady three-dimensional computations. In the present work, AZTRAN is generalized to allow for supersonic freestream Mach numbers.

Earlier development of the ATRAN2 code by Goorjian and his associates at NASA Ames Research Center also has the unified feature of treating subsonic/supersonic flows.[4] Both the AZTRAN code and the ATRAN2 code are based on the framework of the LTRAN2 code developed by Ballhaus and Goorjian.[10]

Other works in extending LTRAN2 to the higher frequency range include the GTRAN[11] and XTRAN2L.[12,13] The latter work also provides a unified scheme for computations of subsonic/supersonic flows. However, in these works thorough assessment of the high-frequency effects appears to be lacking.

The governing equation for AZTRAN and ATRAN2 are basically the low-frequency transonic small-disturbance equations (TSDE), namely,

$$[(M_\infty^2 - 1) + (\gamma + 1)M_\infty^2 \phi_x]\phi_{xx} - \phi_{zz} - 2M_\infty^2 \phi_{xt} = 0 \qquad (1)$$

However, AZTRAN has several improved features over ATRAN2:

1) *Pressure input.* The TES method is known for its efficiency and cost-effectiveness for the computation of unsteady transonic three-dimensional flow for wing planforms.[6,7] Essential in the TES method is that steady pressure inputs are required, instead of the given wing-thickness distribution, for obtaining equivalent airfoil sections along the wing span. A design option in AZTRAN is therefore required in order to perform for the inverse airfoil design. For this purpose, an IAF2 scheme (Inverse AF2) was developed for inverse airfoil design. According to Fung and Chung's procedure,[8] the IAF2 scheme is now unified to include supersonic freestream cases based on the TSDE. The scheme obtains the steady flowfield

Presented as Paper 87-0852 at the AIAA/ASME/ASCE/AHS 28th Structures, Structural Dynamics, and Materials Conference, Monterey, CA, April 6–8, 1987; received Aug. 3, 1987; revision received April 10, 1989. 

*Research Assistant, Mechanical and Aerospace Engineering.
†Associate Professor, Aerospace and Mechanical Engineering. Member AIAA.

and a related equivalent airfoil slope corresponding to a given steady pressure distribution provided either by measurements or by other computational means. This way, the accuracy of the steady mean flow on which the unsteady disturbances propagate is not affected by the small-disturbance and the inversed assumptions. For example, with the design option, AZTRAN can input the shockless pressure distribution of a supercritical airfoil and yield accurate unsteady flow results. Without this option, other codes using TSDE as mentioned above would result in erroneous predictions in both steady and unsteady shock locations.

2) *Characteristics far-field condition.* Several options exist in AZTRAN in coping with the proper far-field boundary condition. In particular, an interpolated characteristics boundary condition was implemented in the supersonic far field.

Let $j = J$ be the far-field boundary line in the $z$ direction. A grid aspect ratio $\lambda$ is introduced, i.e.,

$$\lambda = \frac{\Delta Z_j}{\Delta X_i} \frac{(M_\infty^2 - 1)}{\tau^{2/3}}$$

where $\Delta Z_j$ and $\Delta X_i$ are the height and the width of the grid spacing. When aligned with the characteristic direction, proper values of $\phi$ at the far-field boundary $j = J$ can be evaluated according to the following interpolation scheme, i.e.,

$$\phi_{i,J} = (1-\lambda)\phi_{i,J-1} + \lambda\phi_{i-1,J-1}, \quad \text{for } \lambda < 1 \tag{2a}$$

$$\lambda\phi_{i,J} = (\lambda-1)\phi_{i-1,J} + \phi_{i-1,J-1}, \quad \text{for } \lambda > 1 \tag{2b}$$

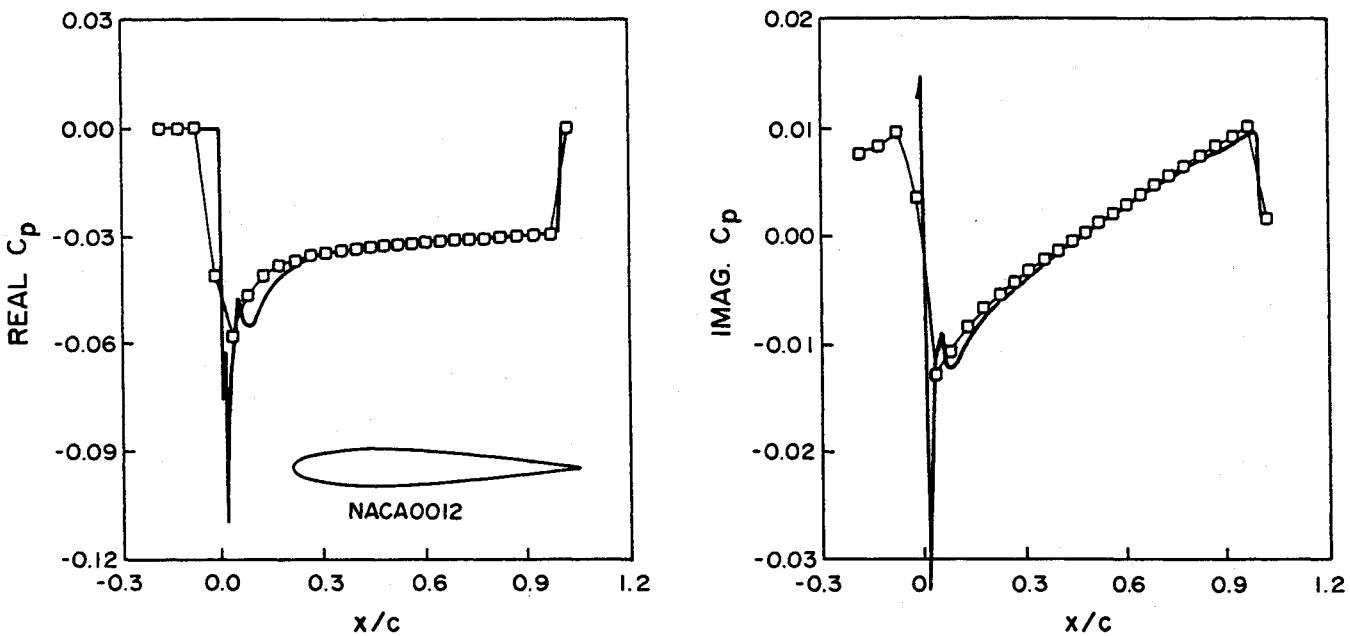


**Fig. 1 In-phase and out-of-phase pressures of NACA 0012 airfoil (upper surface). Pitching oscillation about the quarter-chord at Mach number $M_\infty = 1.05$ and reduced frequency $k = 0.5$. (-□-: present AZTRAN;——: ATRAN2 code.)**

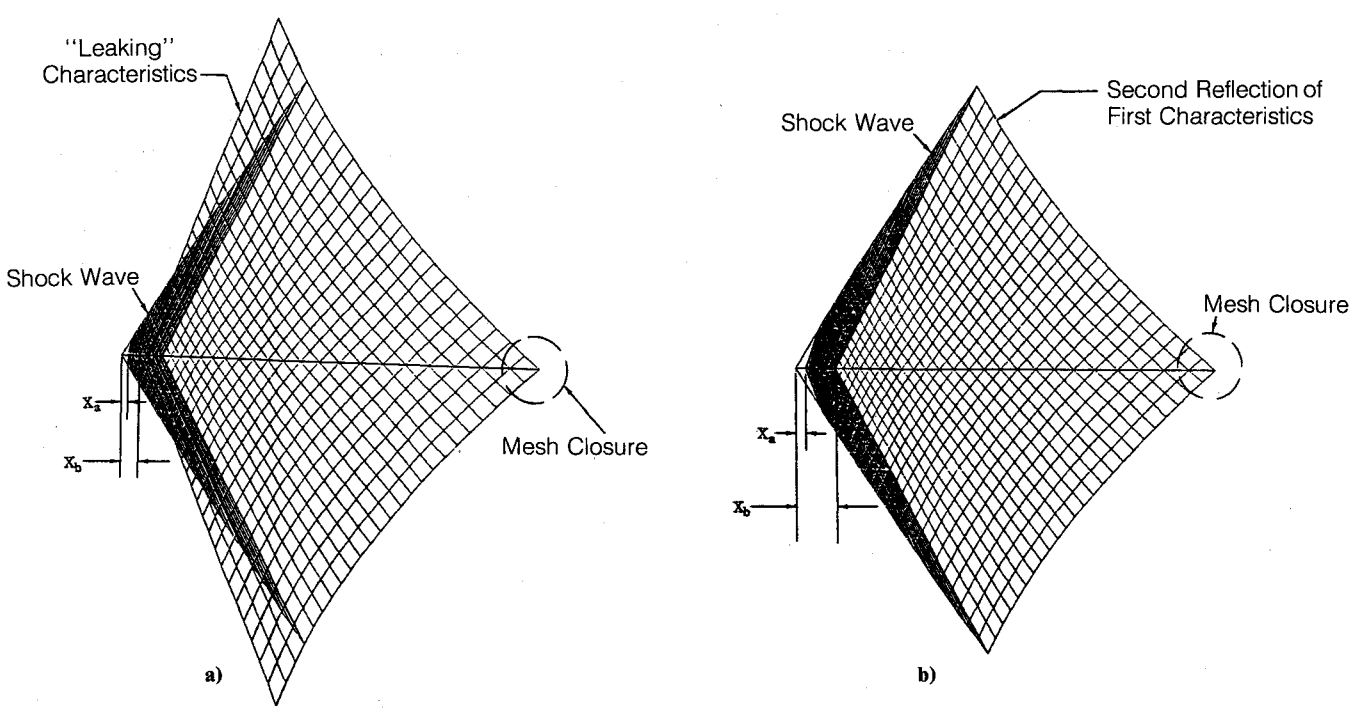


**Fig. 2 Characteristics meshes at $M_\infty = 1.37$ for a 6% parabolic arc airfoil: a) CASCADE code, and b) TMOC code.**

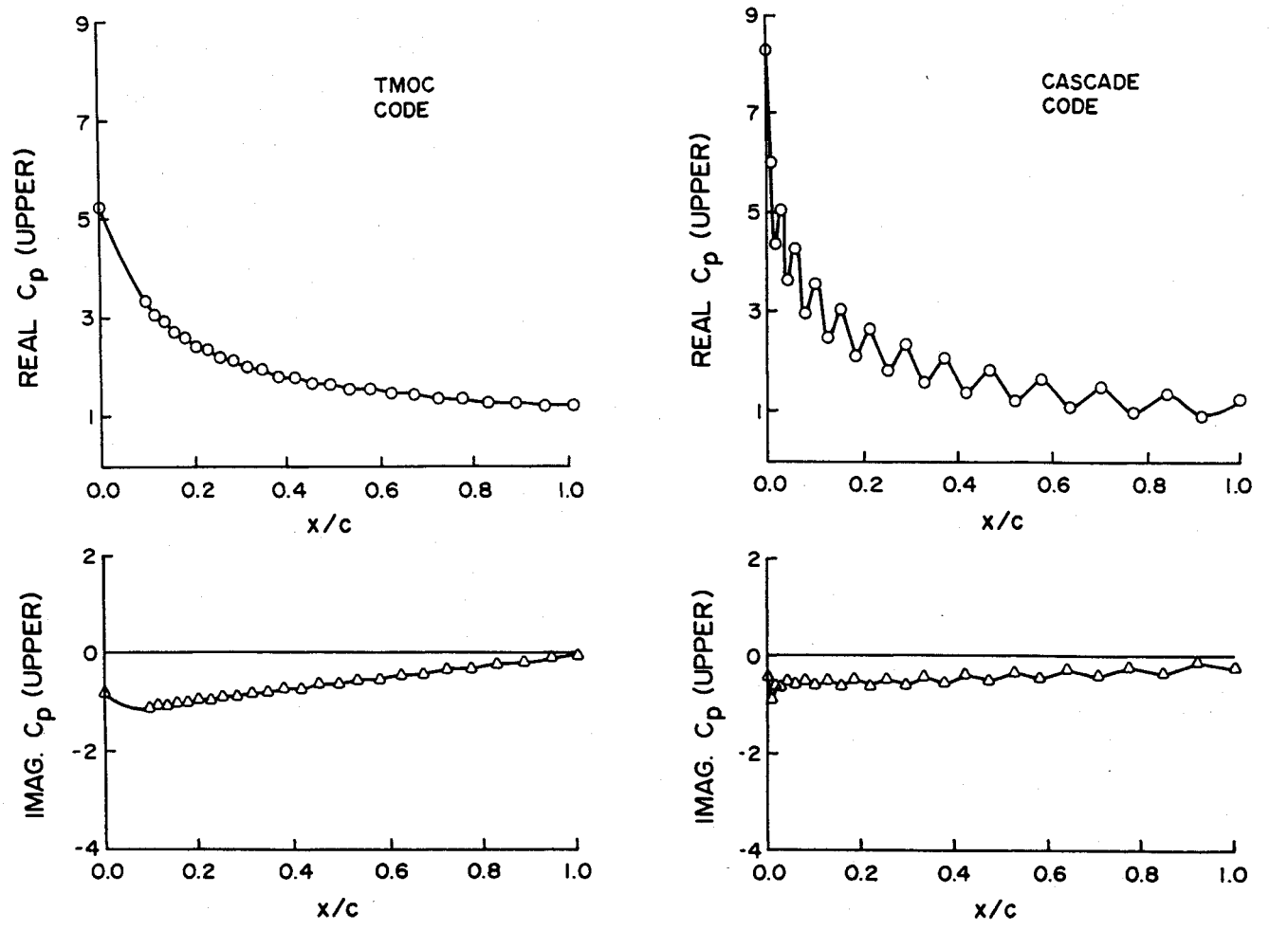


**Fig. 3 Comparison of unsteady pressure results based on the CASCADE code and the TMOC code at near-detachment Mach number $M_\infty = 1.37$ and reduced frequency $k = 0.1$ for a 6% parabolic arc airfoil pitching about the quarter-chord.**

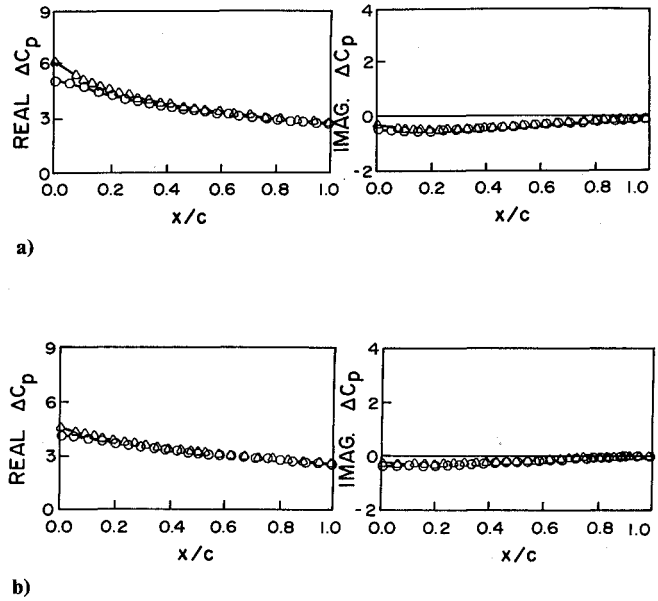


**Fig. 4 Comparison of in-phase and out-of-phase pressure for a 6% parabolic arc airfoil using two nonlinear methods. Pitching oscillation about the quarter-chord at reduced frequency $k = 0.2$ for cases: a) $M_\infty = 1.45$; and b) $M_\infty = 1.55$. (-o-: present AZTRAN; -Δ-: present TMOC.)**

Thus, the reflective waves can be effectively eliminated at the far-field boundaries.

We found that this procedure leads to a more rapid convergence for shock-attachment cases than using the far-field algorithm proposed by Chow and Goorjian.[4] For a typical case, AZTRAN requires 80 CPU seconds in an IBM 3081, whereas ATRAN2 requires nearly three times as much.

3) *Grid spacing.* Ordinarily, AZTRAN adopts a grid system with 103 points in the $x$ direction and 97 points in the $z$ direction. The computational domain is confined to one between 176 chords upstream from the leading edge and 185 chords downstream from the trailing edge in the streamwise direction, and 398 chords each above and below the airfoil in the transverse direction. The airfoil is represented by a slit, along which 23 grid points are distributed in nearly equal spacing. Outside of the airfoil slit, the grid spacing in the streamwise direction is assigned by a mild stretching according to a spacing ratio $\Delta x_i/\Delta x_{i+1} \cong 1.2 \sim 1.4$. Gradual stretching of the mesh size from the slit to the lateral far field, similar to the ZMESH assigned in ATRAN2, is adopted in the transverse direction.

In so doing, AZTRAN captures the proper leading-edge behaviors for in-phase and out-of-phase pressures, whereas ATRAN2 results show highly oscillatory behavior there for a NACA 0012 airfoil (see Fig. 1).

### Development of TMOC

Based on Teipel's original work in nonlinear method of characteristics,[14] Platzer and associates developed the CASCADE code for treatment of oscillating cascades in nonlinear supersonic flow with attached shock waves.[15,16] Their method con-

sists of solving the steady and the time-linearized unsteady TSDE in a sequential manner.

To solve for the steady TSDE, the nonlinear characteristics and compatability relations are employed, i.e.,

$$\left(\frac{dy}{dx}\right)_{ch} = \pm\frac{1}{\sqrt{\lambda}} \tag{3}$$

Here, the dual sign represents the right and left running characteristics along which $\lambda^{3/2} \pm \mu = \text{constant}$, and

$$\lambda \equiv M_\infty^2 - 1 + (\lambda+1)M_\infty^2\phi_{ox}, \qquad \mu \equiv 3/2(\lambda+1)M_\infty^2\phi_{oz}$$

With given initial data, a steady flow can be solved very rapidly. The nonlinear characteristic grid system is then fixed and ready for unsteady flow computations.

Our present efforts in improving the CASCADE code include the following:

1) *Pressure input.* An inverse airfoil design option has also been developed to adopt any given pressure distribution as an input. The pressure coefficient is related to the streamwise velocity by the familiar formula, $\phi_{ox} = -C_p/2$, on the body surface, and the body slope is obtained by the flow tangency condition, i.e., $f'(x) = \phi_{oz}$ at $z = 0$. Thus, an equivalent airfoil can be generated accordingly.

2) *Near-detachment computations.* Because of an improper formulation of the characteristic reflections along the shock front, the CASCADE found to produce oscillatory pressures at the near-shock-detachment Mach numbers. To remedy this deficiency, the present improved formulation requires one to impose a "no-leak" condition on the shock front. The no-leak condition requires that all left-running characteristics are allowed to reflect from the shock boundary only once, except the first characteristics, originating from $x_a$, whose second reflection arrives precisely at the trailing edge (see Fig. 2). Hence, the so-called "mesh-closure" can be achieved at the trailing edge.

To generate the characteristics mesh, two parameters must be specified, namely, $x_a$ and $\Delta$. The parameters $x_a$ and $\Delta$ represent the location of the first characteristics downstream of the leading edge and the increment indicating characteristics spacing, respectively (Fig. 2). The mesh-generation procedure used in CASCADE[15,16] only suggests using small values of $x_a$ and $\Delta$ so long as they satisfy the mesh closure. But no relation is provided for $x_a$ and $\Delta$. However, following Chadwick's selection rule of $x_a$ and $\Delta$ in CASCADE[3] is not sufficient at the near-detachment Mach number. Such a selection often leads to multiple characteristic reflections, all of which must satisfy the mesh-closure condition. Consequently, the majority of the left-running characteristics are found to "leak" out of the shock point, hence the computational domain (see Fig. 2). The leak-out characteristics then carry incorrect values of $\lambda$ and $\mu$ from the freestream, which results in erroneous values in velocities $u$ and $v$ and thus the pressure oscillation on the airfoil.

The no-leak condition imposed by the present method amounts to a numerical process described as follows. An iteration procedure is developed between the chosen parameter $x_a$ and $\Delta$, which is defined as

$$\Delta = (x_b - x_a)/n$$

where $n$ is the number of characteristics emanating from the airfoil, and $x_b$ is the location of the first characteristics reflection on the airfoil. The value of $x_a$ is updated until the no-leak condition is exactly satisfied. As a result, the pressure oscillation is then totally eliminated by this no-leak condition (see Fig. 3). Extensive studies show that the improved code is a robust one valid for any supersonic Mach number, so long as the shock-attachment criterion is assured.

The improved code is called TMOC (transonic method of characteristics). Both CASCADE and the present TMOC codes are governed by the full-frequency time-linearized equation, i.e.,

$$(M_\infty^2 - 1)\phi_{1xx} - (\gamma+1)M_\infty^2(\phi_{1x}\phi_{ox})_x + \phi_{1zz} - 2ikM_\infty^2\phi_{1x} + k^2M_\infty^2\phi_1 = 0 \tag{4}$$

where $\delta\phi_1 = \phi - \phi_o$, and $\delta = \delta_o e^{ikt}$ with $\delta_0$ being the amplitude, and $k$ the reduced frequency based on the full chord. The applicability of TMOC is therefore confined to shock-attachment cases with small amplitude oscillation. Since the present approach is formulated in characteristic coordinates, the grid

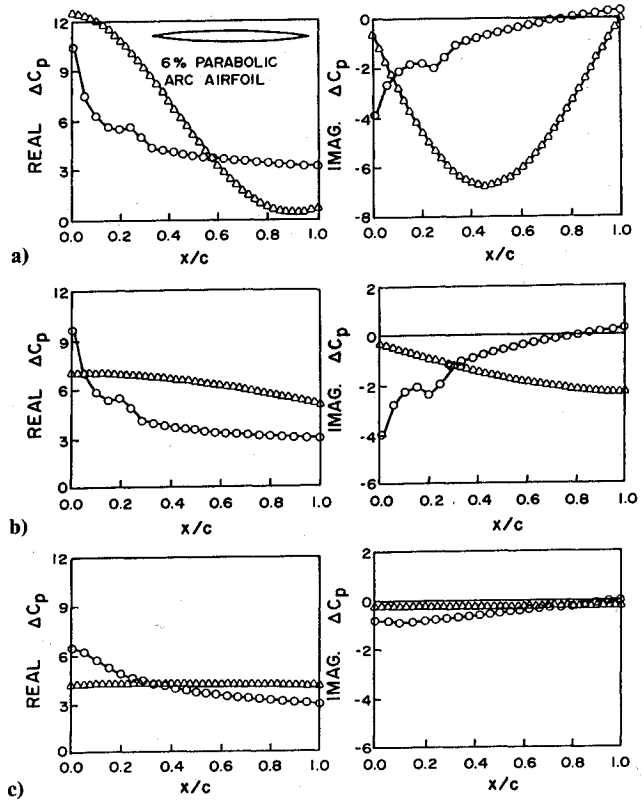


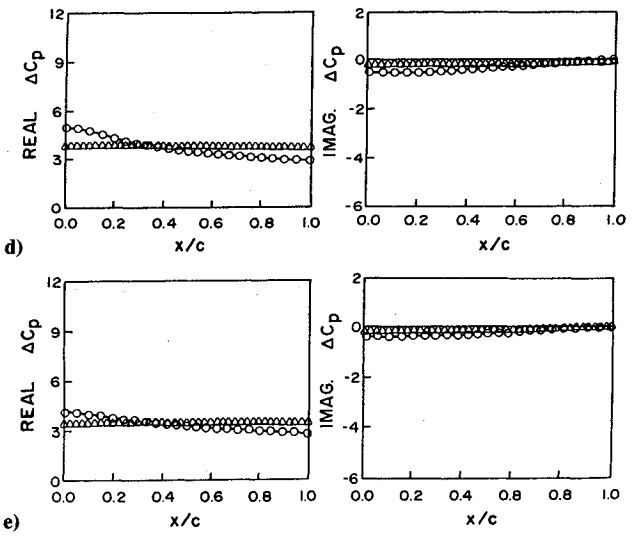


**Fig. 5 In-phase and out-of-phase pressures for a 6% parabolic arc airfoil. Pitching oscillation about the quarter-chord at reduced frequency $k = 0.2$ and at various Mach numbers: a) $M_\infty = 1.05$; b) $M_\infty = 1.15$; c) $M_\infty = 1.37$; d) $M_\infty = 1.45$ (shock attachment); and e) $M_\infty = 1.55$. (-o-: present AZTRAN; -△-: linear theory/LPP.)**

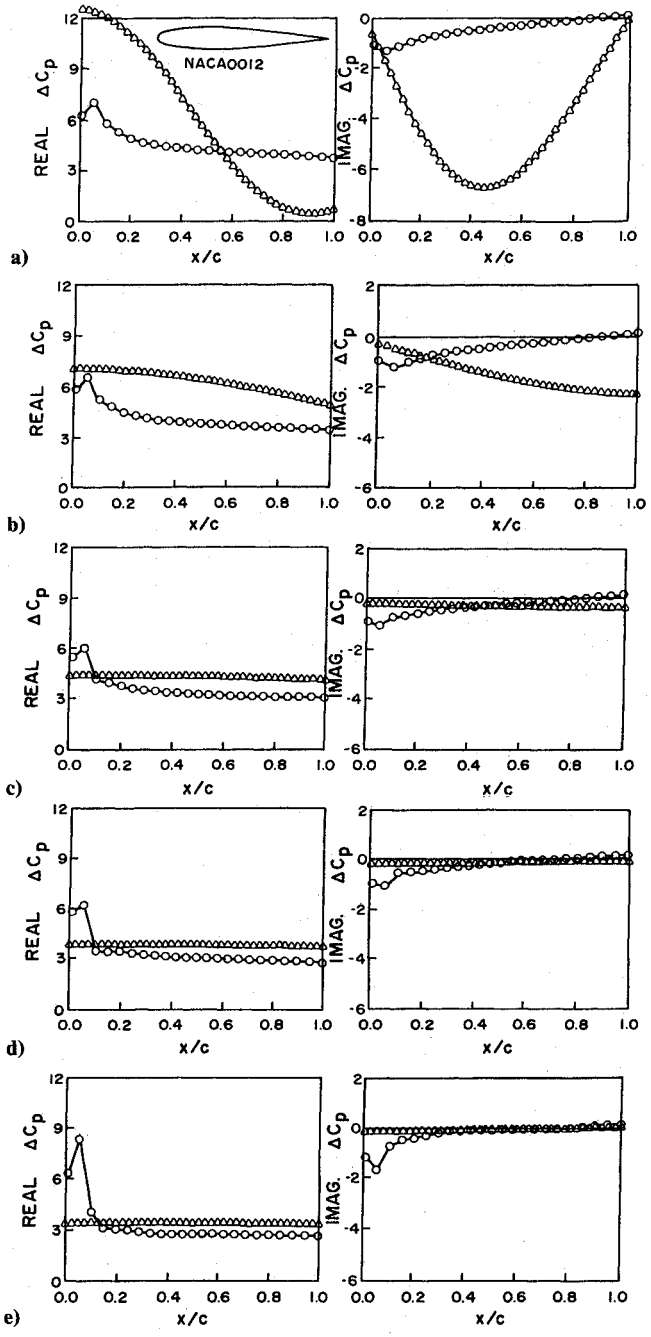


Fig. 6 In-phase and out-of-phase pressure for a NACA 0012 airfoil. Pitching oscillations about the quarter-chord at reduced frequency $k = 0.2$ and at various Mach numbers: a) $M_\infty = 1.05$; b) $M_\infty = 1.15$; c) $M_\infty = 1.37$; d) $M_\infty = 1.45$ (shock attachment); and e) $M_\infty = 1.55$. (-o-: present AZTRAN; -△-: linear theory/LPP).

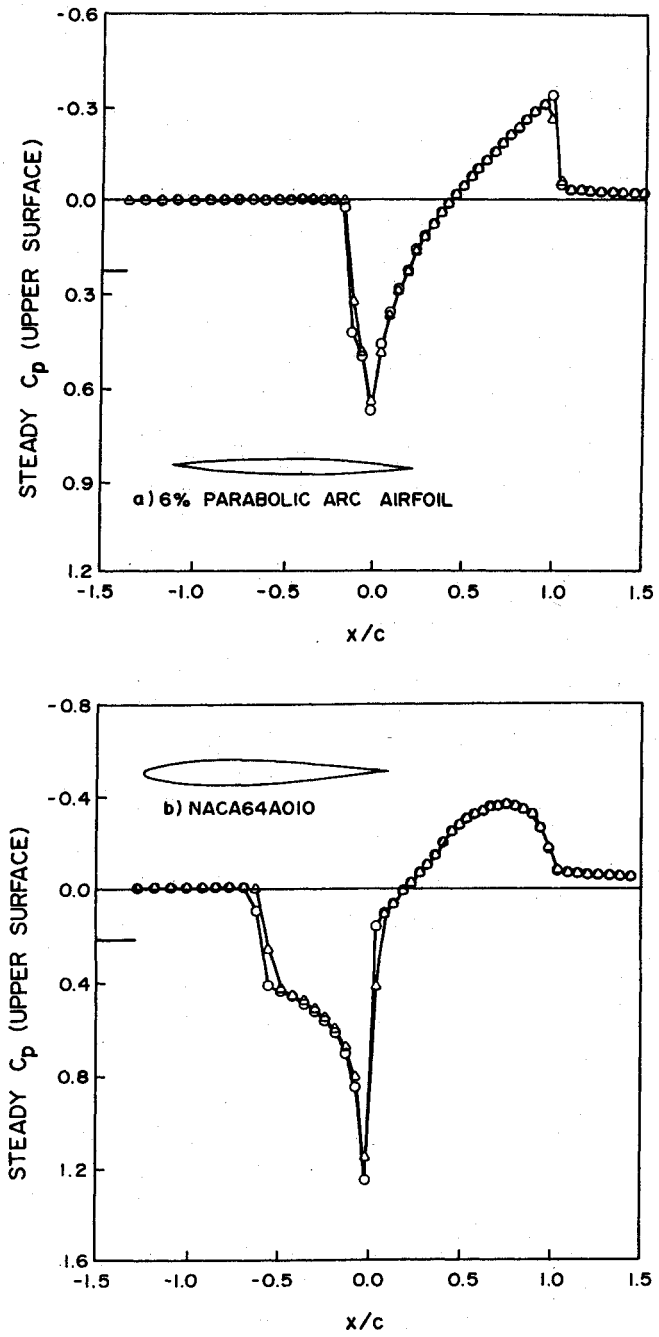


Fig. 7 Inverse airfoil design using AZTRAN: steady pressure inputs and equivalent airfoil pressure outputs for: a) a 6% parabolic arc airfoil; b) a NACA 64A010 airfoil. (-o-: AZTRAN/analysis pressure input; -△-: AZTRAN/design equivalent airfoil output.)

spacing and the flow solution should, therefore, be considered as an exact formulation.

### Cases of Shock Attachment: AZTRAN vs TMOC

To validate the AZTRAN in the realm of shock-attachment Mach numbers, its results are compared with those of TMOC for an oscillating parabolic-arc airfoil (6% thick) at two Mach numbers. Figure 4 shows that the agreement between these two unsteady results becomes closer as the freestream Mach number increases. This is expected since the transonic nonlinearity gradually diminishes with increasing Mach number (also see Figs. 5 and 6).

## Results and Discussion

### Inverse Airfoil Design: Pressure Input

In order to test the inverse airfoil design procedure, the design option IAF2 scheme of the AZTRAN code is used to compute the equivalent airfoil pressure outputs, as shown by the open triangles in Figs. 7 and 8. The pressure inputs, as denoted by open circles, are computed by the analysis option of AZTRAN based on a 6%-thick parabolic arc airfoil and a NACA 64A010 airfoil at $M_\infty = 1.15$. It is seen that slight discrepancies are found at the detached shock location; however, almost identical steady pressures are recovered on the airfoil surfaces for both cases (Figs. 7 and 8). For unsteady pressure

computations, again good pressure recoveries are achieved according to the equivalent airfoils obtained. These unsteady pressure outputs are read from the fifth cycle of the airfoil oscillation.

Next, the inverse airfoil design option of the TMOC code is tested (Fig. 9). This time we use the steady pressure distribution measured by Lessing et al.[17] at three spanwise locations of a rectangular wing at $M_\infty = 1.3$ as the pressure input, denoted by open circles. It is seen that the TMOC inverse design option results in excellent pressure output as denoted by the solid line.

#### Airfoils in Pitching Motions

Figures 4 and 5 show computed unsteady pressure distribution in the real and imaginary components of a 6% parabolic arc airfoil and of a NACA 0012 airfoil in pitching oscillations. In these figures, the AZTRAN results are compared with the results generated by the linear pressure panel (LPP) method based on the linear theory.[18] Several observations can be made from the present study.

First, the detached shock location approaches the airfoil leading edge very rapidly as the freestream Mach number increases starting from the near-sonic flow. Although the shock remains detached at all Mach numbers for the NACA 0012 airfoil, the shock-attachment state for the parabolic arc airfoil is reached rapidly as Mach number increases from 1.05 to 1.37.

Second, for unsteady pressures to approach the linear results, overall agreement can be reached only if the local flow becomes all supersonic, i.e., for shock-attachment cases only. However, such convergence behavior is not to be expected for a blunt leading-edge airfoil such as the NACA 0012 airfoil (see Fig. 6). Since the shock will remain detached from the leading edge, there always exists a small, locally subsonic region in the proximity of the leading edge. As a result, the flow there will continue to affect the unsteady pressure leading to a slow, nonuniform degeneration to the linear results.

#### Comparison with Measured Data

Figures 10 and 11 show a comparison between measured data[19] in the stiffness derivative $C_{m_\theta}$ and the damping-moment derivative $C_{m_{\dot\theta}}$ of a pitching NACA 64A010 airfoil and the computed results of AZTRAN. The pitching axis is located at quarter-chord and the oscillation frequency is 70.6 Hz. It is seen that fairly good agreements are found for both coefficients. It is also interesting to observe that these derivatives are rather insensitive to the changes in the Mach number considered.

#### Flutter Calculations

We have employed both AZTRAN and TMOC for flutter analyses of two different airfoils. Cases of bending and torsion flutters are studied based on the structural parameters given by Isogai (case A of Ref. 20).

In Figs. 12 and 13 (Isogai's case A), the elastic axis is located half-chord upstream of the airfoil ($a = -2.0$) and the natural frequency ratio is selected at $\omega_h/\omega_\alpha = 1.0$ such that flutter is susceptible to occur. Other given parameters are the mass ratio

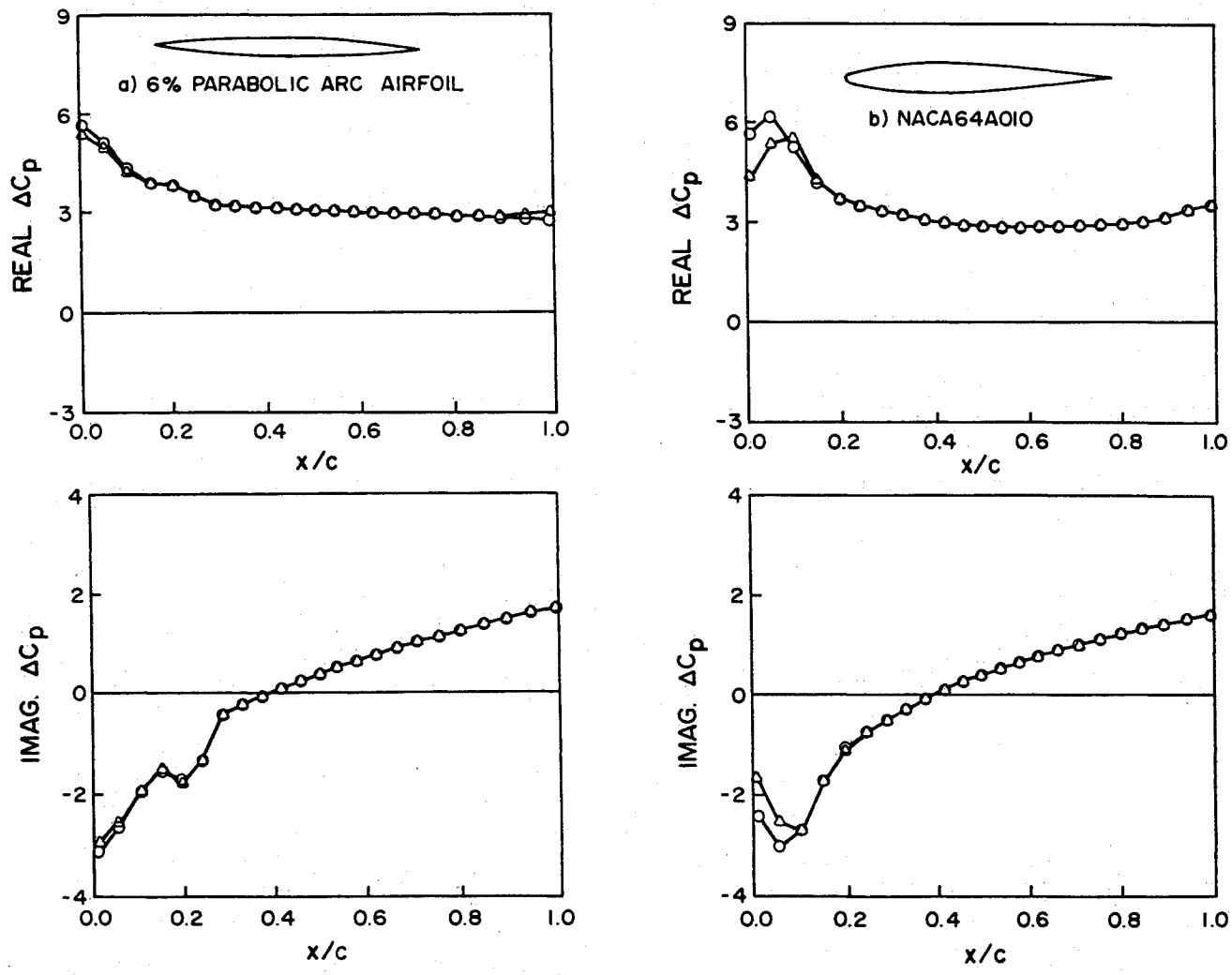


**Fig. 8 Inverse airfoil design using AZTRAN: unsteady pressures for: a) a 6% parabolic arc airfoil; b) a NACA 64A010 airfoil. Pitching oscillations about the quarter-chord at Mach number $M_\infty = 1.15$ and reduced frequency $k = 0.5$. (-o-: AZTRAN/analysis pressure input; -Δ-: AZTRAN/design equivalent airfoil output.)**

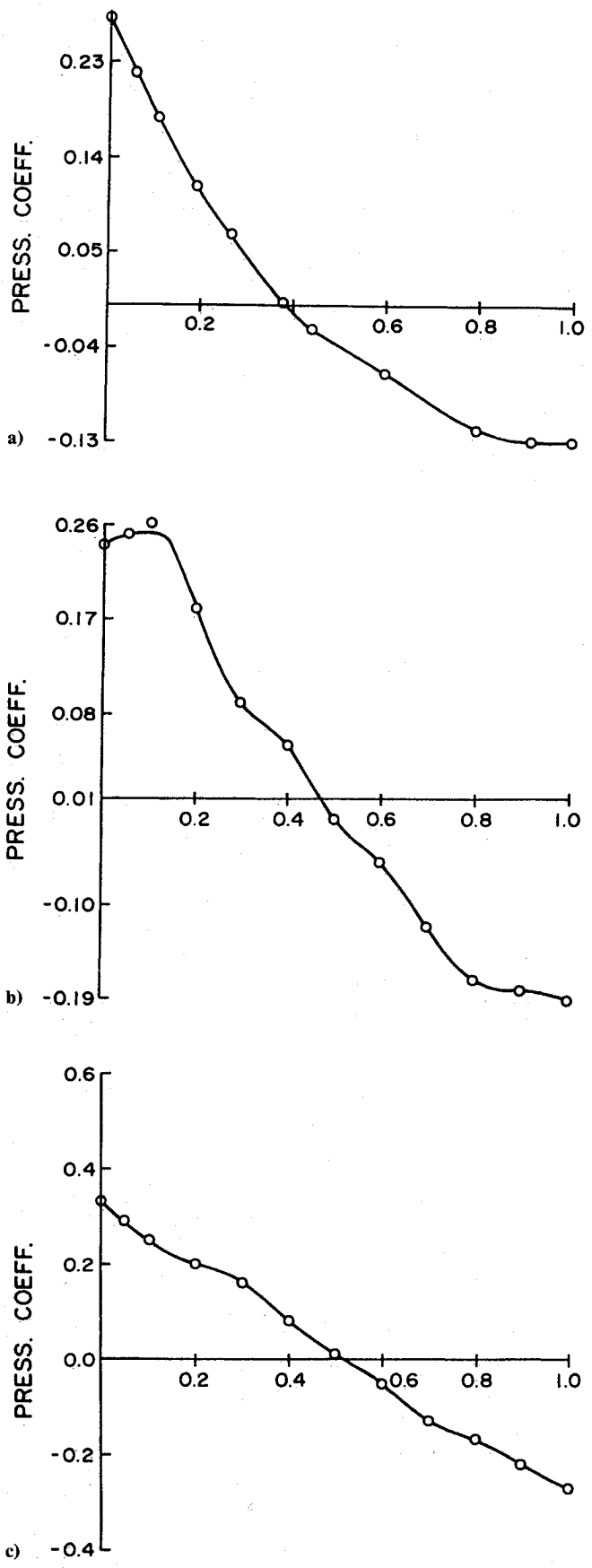


**Fig. 9 Inverse airfoil design using TMOC: steady pressure inputs and equivalent airfoil pressure outputs. Inputs taken from measured data[14] for a rectangular wing at three spanwise locations: a) 50% semispan; b) 70% semispan; and c) 90% semispan at freestream Mach number $M_\infty = 1.3$. (○: measured data; ——: present TMOC equivalent airfoil pressure output.)**

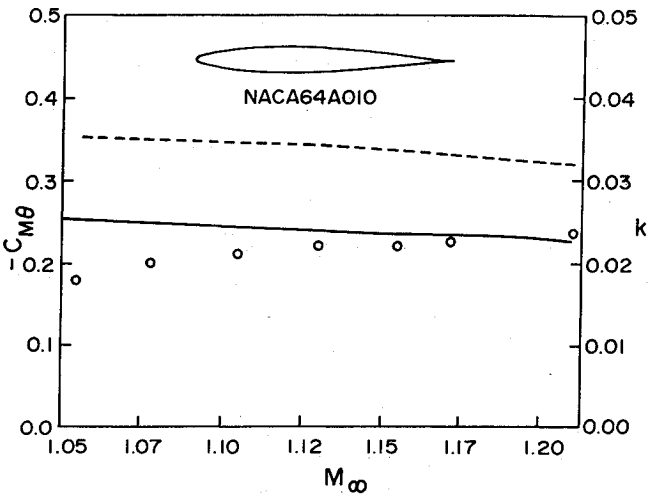


**Fig. 10 In-phase moment coefficients vs freestream Mach numbers. Comparison of computed results with measured data.[16] (○: measured data; ——: present AZTRAN; ---; reduced frequency at $\omega = 70.6$ Hz.)**

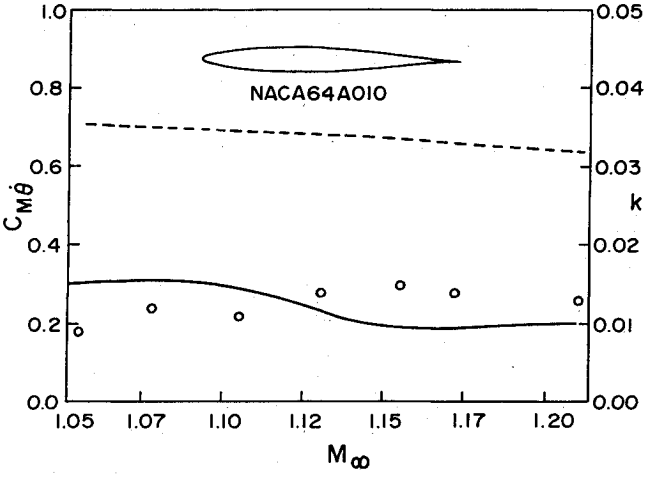


**Fig. 11 Out-of-phase moment coefficients vs freestream Mach numbers. Comparison of computed results with measured data[16] (○: measured data; ——: present AZTRAN; ---: reduced frequency at $\omega = 70.6$ Hz.)**

$\mu = 60$, the static imbalance $x_\alpha = 1.8$, and the radius of gyration $r_\alpha^2 = 3.48$ (notations based on Ref. 18). Two airfoils of equal thickness are considered with the same structural parameters: a 6% parabolic arc airfoil (Fig. 12) and a NACA 64A006 airfoil (Fig. 13).

In Fig. 12, two sharp dips of the flutter boundary are predicted in the upper transonic regime. The first dip occurs around $M_\infty \cong 1.37$. We notice that the latter happens to be near the attachment Mach number ($M_\infty = 1.37$). No flutter is predicted beyond $M_\infty = 1.40$.

The TMOC result appears in fair agreement with that of AZTRAN but shows a steeper flutter boundary. No flutter is predicted before $M_\infty = 1.37$ and beyond 1.38. There is a slight deviation in the flutter-frequency prediction; however, the flutter reduced frequency maintains in the neighborhood of $k \cong 0.2$.

In Fig. 13, a more severe flutter dip is predicted around $M_\infty \cong 1.1$. The flutter speed rapidly increases thereafter until no flutter is predicted around $M_\infty \cong 1.50$. Again, the flutter reduced frequency stays within the proximity of $k \cong 0.2$.

## Computation Time

In running the AZTRAN code, we used typically $103 \times 97$ grid points and 240 time steps for each cycle. Fourier analysis

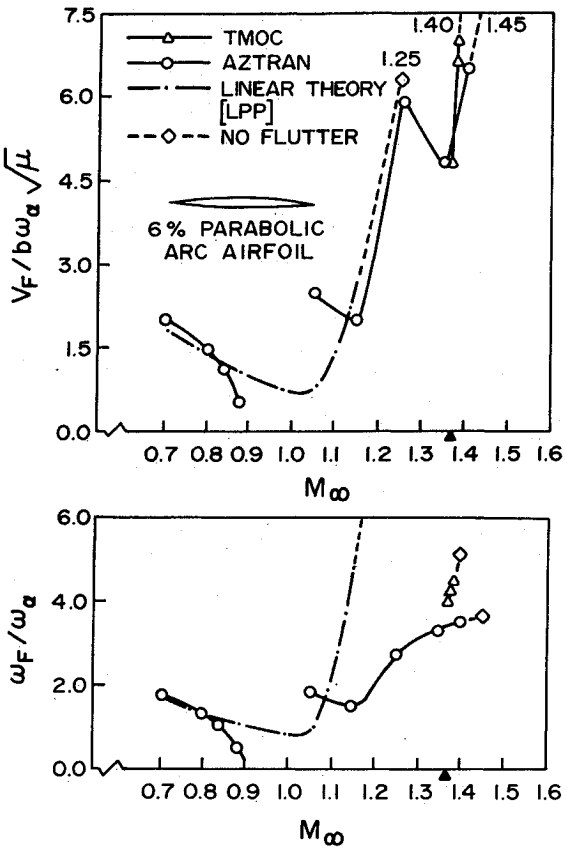


**Fig. 12 Flutter speeds and frequencies vs Mach numbers for a 6% parabolic arc airfoil at zero mean angle of attack. ($\mu = 60$, $\omega_h/\omega_\alpha = 1.0$, $x_\alpha = 1.8$, $r_\alpha^2 = 3.48$, and $a = -2.0$.)**

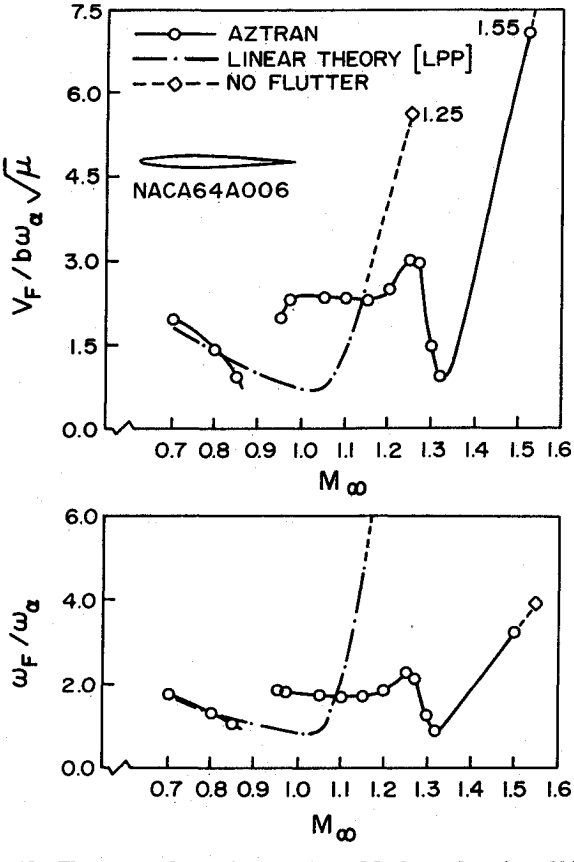


**Fig. 13 Flutter speeds and frequencies vs Mach numbers for a NACA 64A006 airfoil at zero mean angle of attack. ($\mu = 60$, $\omega_h/\omega_\alpha = 1.0$, $x_\alpha = 1.8$, $r_\alpha^2 = 3.48$, and $a = -2.0$.)**

of pressure data is performed usually in the third cycle. Typically, it takes 100–500 iterations for detached-shock cases and 40–60 iterations for attached-shock cases in order to reach a satisfactorily converged steady flow. On an IBM 3081, the CPU time ranges from no more than 600 s to as few as 45 s, respectively, for a complete steady and unsteady flow computation. However, as the freestream Mach number approaches sonic, say 1.05, the number of iterations required for convergence would increase to 2000. In this case, the CPU time would increase to around 800 s.

By contrast, the TMOC code requires only a couple of seconds in CPU time for a complete case of computation. Since the formulation is exact and the grid points fixed except in determining parameters $x_a$ and $\Delta$, no further iteration is needed.

## Conclusions

Comprehensive studies of two developed transonic methods for oscillating airfoils in the upper transonic Mach numbers are presented. Both methods have the inverse airfoil design option in that an equivalent airfoil can be generated according to a given pressure input. Computed results of these methods are verified with each other and with those of the ATRAN2 code, the linear theory, and measured data.

Based on our computed results, some conclusions can be drawn.

1) Clearly, the upper transonic dips in the flutter boundaries have a definite relation to the shock patterns (attached or detached). However, the detailed physical interpretation of the transonic dips remains to be further clarified.

2) In the lower transonic range, the flutter results predicted by the linear theory appear to be in fair agreement with those of the transonic theory, as confirmed by the present study. By contrast, our study shows that the flutter results based on the linear theory are not reliable in the upper transonic Mach number range, as they fail to predict the transonic dips. More important, they become less conservative at the lower Mach numbers (1.1–1.3).

Therefore, the present study warrants further investigations in this upper transonic flow regime where the nonlinearity plays an essential role in the unsteady aerodynamics. Further experimental work as well as development of three-dimensional computation methods in this area are recommended.

## Acknowledgments

This work was supported by the Navy/DTNSRDC Contract No. N00167-85-K-0164; T. C. Tai and Greg Huson are the contract monitors. The authors would like to thank Peter Goorjian and Leslie Chow of NASA Ames Research Center for many valuable discussions throughout the course of this research. Permission to use the Cray-XMP for computation by Paul Kutler of NASA Ames is gratefully acknowledged. They also would like to thank Professor Max Platzer of Naval Postgraduate School for providing the CASCADE code and many helpful discussions. Thanks are also due to John Batina of NASA Langley Research Center for providing the XTRAN2 code and the related documents. At Arizona State University, our consultations with P. C. Chen and Pablo Garcia-Fogeda were most helpful for the flutter cases.

## References

[1]Chen, P. C., and Liu, D. D., "A Harmonic Gradient Method for Unsteady Supersonic Flow Calculations," AIAA Paper 83-0887, 1988. Also *Journal of Aircraft*, Vol. 22, May 1985, pp. 371–379.

[2]Kacprzynski, J. J., Ashley, H., and Sankaranarayanan, R., "On the Calculation of Unsteady Nonlinear Three-Dimensional Supersonic Flow Past Wings," *Journal of Basic Engineering*, Dec. 1968, pp. 581–595.

[3]Chadwick, W. R., "Unsteady Supersonic Cascade Theory Including Nonlinear Thickness Effects," Ph.D. Thesis, Naval Postgraduate School, Monterey, CA, June 1975.

[4]Chow, L. J., and Goorjian, P. M., "Implicit Unsteady Transonic Airfoil Calculations at Supersonic Freestreams," AIAA Paper 82-0934, 1982.

[5]Weatherill, W. H., Sebastian, J. D., and Ehlers, E. E., "Application of a Finite-Difference Method to the Analysis of Transonic Flow Over Oscillating Airfoils and Wings," AGARD CP-227, Paper 5, Sept. 1977.

[6]Liu, D. D., "Computational Transonic Equivalent Strip Method for Applications to Unsteady 3D Aerodynamics," AIAA Paper 83-0261, Jan. 1983.

[7]Liu, D. D., Kao, Y. F., and Fung, K. Y., "An Efficient Method for Computing Unsteady Transonic Aerodynamics of Swept Wings with Control Surfaces," *Journal of Aircraft,* Vol. 25, Jan. 1988, pp. 25-31.

[8]Fung, K. Y., and Chung, A., "Computations of Unsteady Transonic Aerodynamics Using Prescribed Steady Pressures," *Journal of Aircraft,* Vol. 20, Dec. 1983, pp. 1058-1061.

[9]Fung, K. Y., "A Simple, Accurate, and Efficient Algorithm for Unsteady Transonic Flow," *Recent Advances in Numerical Methods in Fluid Dynamics,* edited by W. G. Habashi, Pineridge Press, Swansea, UK, 1984, pp. 317-339.

[10]Ballhaus, W. F., and Goorjian, P. M., "Implicit Finite-Difference Computations of Unsteady Transonic Flows about Airfoils," *AIAA Journal,* Vol. 15, Dec. 1977, pp. 1728-1735.

[11]Rezzetta, D. P., and Chin, W. C., "Effect of Frequency in Unsteady Transonic Flow," *AIAA Journal,* Vol. 17, July 1979, pp. 779-781.

[12]Seidel, D. A., Bennett, R. M., and Whitlow, W., Jr., "An Exploratory Study of Finite-Difference Grids for Transonic Unsteady Aerodynamics," NASA TM-84583, Dec. 1982. Also AIAA Paper 83-0233, Jan. 1983.

[13]Whitlow, W., Jr., "A Program for Solving the General Frequency Unsteady Transonic Small Disturbance Equation" NASA TM-85723, Nov. 1983.

[14]Teipel, I., "Calculation of Unsteady Aerodynamic Forces in Transonic Flow," *Journal de Mecanique,* Vol. 4, No. 3, Sept. 1965, pp. 335-360.

[15]Platzer, M. F., and Chalkley, H. G., "Theoretical Investigation of Supersonic Cascade Fluter and Related Interference Problems," AIAA Paper 72-377, April 1972.

[16]Platzer, M. F., Chadwick, W. R., and Schlein, P. B., "On the Analysis of the Aerodynamic and Flutter Characteristics of Transonic Compressor Blades," *Revue Francaise de Mecanique, Numero Special,* 1976, pp. 65-74.

[17]Lessing, H. C., Troutman, J. L., and Menees, G. P., "Experimental Determination of the Pressure Distribution on a Rectangular Wing Oscillating in the First Bending Mode for Mach Numbers for 0.24 to 1.30," NASA TND-344, Dec. 1960.

[18]Liu, D. D., and Pi, W. S., "Transonic Kernel Function Method for Unsteady Flow Calculations Using a Unified Linear Pressure Panel Procedure," AIAA Paper 80-0737-CP, 1980.

[19]Nakamura, Y., and Tanabe, Y., "Some Experimental Contribution on Single Degree-of-Freedom Flutter in Two-Dimensional Low Supersonic Flow," *Journal of Aircraft,* Vol. 3, Sept.-Oct. 1966, pp. 405-410.

[20]Isogai, K., "Numerical Study of Transonic Flutter of a Two-Dimensional Airfoil," National Aerospace Lab., NAL TR-617T, July 1980.

[21]Scanlan, R. H., and Rosenbaum, *Introduction to the Study of Aircraft Vibration and Flutter,* Macmillan, New York, 1951, Chap. 8, p. 194.